Why χ Is Seldom Zero for Polymer−Solvent Mixtures

Scott T. Milner* and Martin-Daniel Lacasse

ExxonMobil Research and Engineering Route 22 East, Annandale, New Jersey 08801

William W. Graessley

74 Old Channel Trail, Montague, Michigan 49437

Received May 15, 2008; Revised Manuscript Received December 15, 2008

ABSTRACT: Typical good nonpolar solvents for nonpolar polymers have values of the Flory interaction parameter χ of 0.3 or higher. This is striking since miscible nonpolar polymer blends exist with well-matched solubility parameters and resulting very small χ values of 10^{-2} or less. Using a cell model, it has been previously argued that there is a generic contribution to χ in polymer−solvent systems of about 0.3, which ultimately arises from the difference in affinity for free volume of bonded chain mers and otherwise identical solvent mers. We explore this result with off-lattice MC simulations of hard-sphere freely jointed chains in identical hard-sphere solvent. We observe reductions in chain radii of gyration and of virial coefficients for dimers among hard-sphere solvents versus in vacuum, consistent with the cell model results. Finally, we extract free volume distributions and observe reduced free volume of chain mers compared to solvent. With a model of a single mer in a fluctuating cell surrounded by hard-sphere fluid, we construct free volume distributions in good agreement with our MC results and previous work of Sastry et al. on hard-sphere liquids.

Introduction

Truly good solvents for polymers are hard to come by. This maxim has a specific technical meaning in terms of the Flory χ parameter, which measures the strength of repulsive polymer−solvent interactions within the Flory−Huggins theory[1]

$$\beta F = \phi/N \log(\phi/N) + (1 - \phi) \log(1 - \phi) + \chi\phi(1 - \phi) \quad (1)$$

which gives the mixing free energy per segment of a solution of a polymer of N segments and volume fraction ϕ. In this mean-field description of polymer−solvent interactions, χ measures the strength of repulsive interactions between polymer and solvent segments. (In this paper, a solvent molecule is defined to consist of a single "segment".)

Absent specific attractive interactions between polymer and solvent, one might expect χ to be positive (repulsive), in which case the best solvent one could hope for would be "athermal", i.e., with $\chi = 0$. In fact, a perusal of the *Polymer Handbook*[2] is sufficient to persuade oneself that the preponderance of so-called "good" solvents for common polymers actually have χ values upward of 0.3. This behavior of χ for polymer solutions is well-documented[3,4] and has been known for many years.[5−7] This behavior is illustrated for common good solvents of polyethylene in Figure 1.

This is remarkable because $\chi = 0.5$ is the limiting value for a "marginal solvent", defined such that the excluded volume parameter w for polymer segments vanishes. Upon expanding the free energy density to second order in monomer concentration c, w is defined as the coefficient of the $O(c^2)$ term. Using $c = \phi/\Omega_0$, we have

$$w = \Omega_0(1 - 2\chi) \quad (2)$$

in which Ω_0 is the segment volume. For athermal solvents, w equals Ω_0, which is as large as w can be in the absence of polymer−solvent attractions, which induce effective polymer−polymer repulsions. To say that χ for good solvents is typically 0.3 means w is only 40% of its naive scaling value Ω_0.

* To whom correspondence should be addressed.

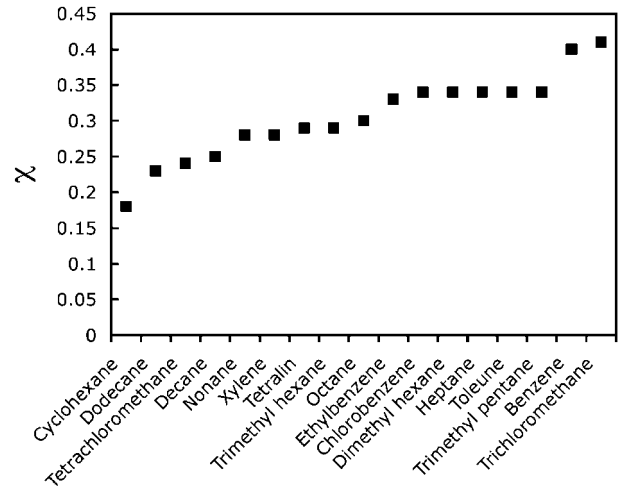

Figure 1. A rank-ordered list of χ values for 17 common good solvents for polyethylene. Nearly all values are at or above 0.3.

This is all the more striking because for polymer−polymer blends χ can can be made extremely small (10^{-2}−10^{-3}) by choosing polymers that are appropriately matched.[8,9] This is fortunate since if it were not the case that χ for polymer blends could be made so small, it would be impossible to make miscible polymer blends, as the threshold for phase separation is χ of order $1/N$.

For blends of polymers without significant polar groups or hydrogen bonding, a good account of the χ parameter can be given in terms of solubility parameters. The underlying physical reason is that repulsions between such polymers arise from dispersive interactions, which are proportional to the product of molecular polarizabilities. This ultimately leads to χ of the form

$$\chi_{ij} = \Omega_0/T(\delta_i - \delta_j)^2 \quad (3)$$

where δ_i is the "solubility parameter" of polymer i (δ^2 has dimensions of energy density).

10.1021/ma801091b CCC: $40.75
Published on Web 01/13/2009

Equation 3 works well for describing, e.g., saturated hydrocarbon random copolymers of various α-olefin monomers.[10,11] In particular, there have been miscible blends predicted and observed based on matching the solubility parameters of chemically dissimilar polymers.[12] Evidently, if the repulsive interaction depends on the square of a difference of parameters, χ can be made to vanish by matching those parameters. In sharp contrast, eq 3 is quoted for polymer−solvent systems as a rule of thumb—with an additive constant of 0.34.[2]

There are several important consequences of typical values of w being so much smaller than the athermal limiting value of Ω_0.[13] First of all, a single chain in solution will have a smaller coil dimension than one naively expects on the basis of scaling ($w \sim \Omega_0$). Flory gave an account of the swelling of a single chain in solvent.[14] We briefly reprise Flory's argument in the Appendix. The main result is that the mean-square end-to-end distance R is given by

$$(R/R_0)^5 - (R/R_0)^3 = (1/2)(N/N_s)^{1/2} \tag{4}$$

in which R_0 is the mean-square end-to-end distance of the same chain in a melt. Here N_s is a crossover "swelling molecular weight", given by $N_s = b^6/w^2$ (here b is the statistical segment length, such that $R_0^2 = Nb^2$). For chains shorter than N_s, eq 4 gives chain dimensions similar to R_0—the chain is too short to swell in the solvent.

Since w is typically smaller than Ω_0, whereas b^3 is typically somewhat larger than Ω_0, the swelling chain length N_s is typically large compared to unity. This means that chain dimensions in dilute solution are smaller than one might expect. This likewise increases the "overlap concentration" at which individual chains begin to fill space and overlap. Smaller coils in semidilute solution means fewer entanglements between chains, i.e., a larger molecular weight per entanglements.

Finally, if we increase the concentration of a solution beyond a certain "swelling concentration" ϕ_s, we arrive at a situation in which chain self-avoidance is no longer relevant, and chain configurations are Gaussian as in the melt. Above ϕ_s, a chain segment large enough to benefit from self-avoidance no longer dominates the average concentration in its immediate vicinity; that is, most of its repulsive interactions are with other chains. Therefore, self-avoidance cannot help in reducing a chain's repulsive interactions; the chain may as well be Gaussian and maximize its entropy. The existence of a significant range of concentration over which chains are Gaussian (typically down to $\phi_s = 0.1$ or so) is a consequence of the small value of w.

All of which begs the question, why is it so hard to find a truly good solvent? What could be the origin of the extra repulsive interaction beyond the dispersive term summarized in eq 3? One might reflexively respond that the additional contribution must be of entropic origin; how do we identify more precisely what that means?

The physical origin of the additional contribution to χ has been argued to arise from the behavior of the thermal expansion coefficient for typical nonpolar polymers as opposed to solvents.[15,16] It has been noted that the values for the polymers and solvents are practically nonoverlapping;[16] the polymer values are clustered around 7×10^{-4}/K, while the solvent values are clustered around 12×10^{-4}/K, a factor of about 1.7 larger.[2,17]

This contrast in thermal expansion coefficients suggests that solvent molecules rattle about more aggressively than do polymer segments, in exploring the available "free volume". This is natural within a simple picture in which the segments of a polymer are physically identical to a single solvent molecule but are covalently bonded into chains, so that the mers of a polymer have fewer translational degrees of freedom than do unbonded solvent mers. Within a freely jointed chain model, each additional chain mer brings two degrees of freedom, while an unbonded solvent molecule would have three degrees of freedom.

Now this tendency to explore free volume to a greater or lesser extent has consequences for the state of a pure solvent or polymeric liquid. The configurational entropy is increased by increasing the free volume, but the cohesive energy is reduced; there exists an optimum free volume at a given temperature. Consider a simple case in which solvent molecules and polymer segments are identical—i.e., have the same attractive interactions between units and the same hard-core volume—differing only because of the effect of polymeric bonds in reducing the number of degrees of freedom for the polymer segments. One would expect the optimum free volume for the pure solvent liquid to be larger than for the pure polymer liquid because of the stronger influence of configurational entropy of the solvent.[18]

In a polymer−solvent mixture, a compromise value of free volume per segment would be reached. Compromise is always painful; thus, the mixing free energy would have positive contributions from the both the configurational entropy and the cohesive energy, which would compete with the positive entropy of mixing that always drives miscibility. The resulting mixing free energy interpreted in terms of χ would then have a positive contribution from a proper accounting for configurational entropy.

A calculation of this entropic contribution to χ has been given by Patterson,[15] employing the cell model of configurational entropy developed by Prigogine,[19] extended by Flory, Orwoll, and Vrij (FOV)[20−22] to the case of polymer−solvent mixtures. They express χ as the sum of two contributions: an exchange term χ_{exc} of the form of eq 3 associated with the mismatch in component cohesive energy density Π and a free volume term χ_{fv} associated with the mismatch in component thermal expansion coefficient α:

$$\chi = \chi_{exc} + \chi_{fv} \tag{5}$$

Both χ_{exc} and χ_{fv} are in principle positive quantities. For polymer solutions, however, there is a systematic solvent−polymer mismatch in α, with $\alpha_s > \alpha_p$, such that χ_{fv} becomes significant. Patterson used the FOV model to derive the following formula:[15]

$$\chi_{fv} = \frac{\Pi_s V_s \alpha_s}{2R}\left(\frac{T_p^* - T_s^*}{T_p^*}\right)^2 \tag{6}$$

in which V_s is the solvent molar volume and T_p^* and T_s^* are characteristic temperatures of the polymer and solvent, given by

$$T^* = \frac{3}{\alpha}\frac{(1 + 4\alpha T/3)^4}{(1 + \alpha T)^3} \tag{7}$$

The interaction parameter data for a wide range of polymer solutions as well as the significance of the above equations are discussed extensively in ref 34 and in section 7.3 of ref 16. An estimate based on average values of $\Pi_s = 340P$ J/cm^3, $V_s = 100$ cm^3, $\alpha_s = (11.9 \pm 1.8) \times 10^{-4}$ K^{-1}, and $\alpha_p = 6.8pm0.9 \times 10^{-4}$ K^{-1} for a wide range of typical solvents and polymer components leads to $\chi_{fv} \approx 0.3$ and hence to the generic estimate of the minimum χ for polymer solutions given above.

As noted above, the rule of thumb that $\chi > 0.3$ is not a rigid rule. It can be violated for any of four reasons:[16] (1) the action of specific polymer−solvent attractions, (2) the use of oligomeric solvents, (3) polymers with unusually large α_p, and (4) solvents with unusually small α_s.

The first of these is illustrated by solutions of poly(ethylene oxide) in benzene[23] and poly(propylene oxide) in benzene[24] and the second by solutions of polyethylene in a series of *n*-alkanes ($\chi = 0.36$ for C8, progressing to $\chi = 0.29$ for C12).[25] The progression of χ with increasing *n*-alkane carbon number is also consistent with thermal expansion coefficient behavior: α_s decreases with increasing *n*, smoothly approaching the polyethylene value.[26,27] Contributions from χ_{exc} interfered with testing the third possibility. Thus, although $\alpha_p = 9.13 \times 10^{-4}$ K^{-1} for polydimethylsiloxane is near the solvent average (see above), the available χ values for its solutions all lay above 0.40. Consistency with the fourth possibility, however, is furnished by solutions of polyethylene in the cyclic saturated hydrocarbon liquids *cis*-decalin and *trans*-decalin, with $\alpha_s = 8.7 \times 10^{-4}$ K^{-1} and $\alpha_s = 8.9 \times 10^{-4}$ K^{-1}, respectively.[28] Both values displaced significantly toward the polymeric range (see above), and their polyethylene solutions behave accordingly ($\chi = 0.07$ and $\chi = 0.05$, respectively).[25]

In the present work, we have used computer simulations with hard-sphere polymers and solvents to explore the mechanism for free volume contributions to χ_{fv}, without interference from χ_{exc} contributions. We have also developed an simpler alternative formulation of the FOV cell model calculation of χ_{fv}, drawing on the approach of ref 16 but with terminology that lends itself to detailed microscopic interpretations, the main interest in this paper. In the next section, we present our version of a cell model of polymer solvent mixtures.

Cell Model

In a cell model for polymer solutions, each cell is occupied by either a monomeric unit of a polymer chain (component 1) or a solvent molecule (component 2). For solutions of freely joined chains of hard spheres (volume fraction ϕ) in a liquid of identical hard spheres, the exchange interaction is by definition zero, hence $\chi_{exc} = 0$. Each cell, regardless of occupant, has the same volume v, which varies with temperature T and pressure P in such a way as to minimize the free energy. The cells and their contents are otherwise mutually independent.

Aside from some additive constant which drops out of the calculations, the Helmholtz free energy per cell f is the sum of two terms: an entropic contribution representing the exploration of free volume and an energetic contribution corresponding to the cohesive energy density of the liquid. We write the free energy per particle of a cell model as

$$f = -Tc \log(v^{1/3} - v^{*1/3}) - \frac{\epsilon}{v} + f_{mix} \tag{8}$$

The first term in eq 8 represents the configurational entropy associated with each segment moving within its cell. The cell-and-segment geometry is approximated as follows: the cell is taken to be a cube of linear dimension $v^{1/3}$, while the segment within is taken to be a slightly smaller sphere of diameter $v^{*1/3}$, translating independently in the *x*, *y*, and *z* directions. (We may equivalently consider a hard spherical particle of volume v_0 translating within a spherical cavity of volume v.) Hence v^* is the minimum volume per segment within this simple model, achieved in the low-temperature limit. Thus, the first term in eq 8 represents the log of the number of places we can place a segment in its cell.

The coefficient c is the cell fraction weighted average of the Prigogine parameters[19] of the two components:

$$c = c_1\phi + c_2(1 - \phi) \tag{9}$$

The Prigogine parameter counts the number of translational degrees of freedom per segment for each component. For a freely jointed polymer chain of spherical monomers we have $c_1 = 2$; for a solvent of featureless spherical monomers we have $c_2 = 3$.

The second term in eq 8 is a mean-field estimate of the cohesive energy per cell as proportional to the square of concentration, with a coefficient ϵ which is the same for both species. Here ϵ/v^{*2} is the cohesive energy density of the hypothetical "close-packed liquid" (i.e., liquid with negligible free volume, at random close packing), and the $1/v$ dependence echoes the usual mean-field approximation of van der Waals.

The final term f_{mix} is the Flory−Huggins approximation to the ideal mixing free energy per particle

$$f_{mix} = T\frac{\phi}{N_1}\log\frac{\phi}{N_1} + T\frac{1-\phi}{N_2}\log\frac{1-\phi}{N_2} \tag{10}$$

where N_1 and N_2 are the number of segments per molecule in species 1 and 2 (we shall take $N_1 = N$ for the polymer and $N_2 = 1$ for the solvent). In separating this term from the configurational entropy associated with motion within a cell, we are making a physically motivated approximation, in which the mixing of species is a process distinct from the determination of the density.

The pressure is given by the appropriate thermodynamic derivative, $p = -\partial f/\partial v$, with the result

$$p = \frac{Tc}{3v^{2/3}(v^{1/3} - v^{*1/3})} - \frac{\epsilon}{v^2} \tag{11}$$

For a given pressure, the above equation can be solved (numerically) to determine v. For modest pressures, since the internal pressure $\Pi = \epsilon/v^2$ is so much larger than p, it suffices to take $p \approx 0$ in determining v.

The thermal expansion coefficient α is likewise given by the thermodynamic derivative $\alpha = (1/v)(\partial v/\partial T)$. For temperatures well below any critical points, the ratio v/v^* is nearly unity, which allows us to expand the equation of state to obtain $v/v^* \approx 1 + Tc/(\Pi^* v^*)$ from which we see that $\alpha \approx c/(\Pi^* v^*)$, i.e., that α is proportional to c. (Here $\Pi^* = \epsilon/v^{*2}$ is the cohesive energy density of the "close-packed liquid".) Thus, the ratio of thermal expansion coefficients for solvents and polymers with otherwise identical hard-core volumes v^* and cohesive energy densities Π^* would be expected to be about $3/2 = 1.5$, not far from the 1.7 or so suggested by thermal expansion coefficient data for polymers and solvents.

Our goal is to compute a free energy of mixing based on eq 8. To do this, we expand f to second order in the variation of c and all quantities that depend on it (i.e., v). For later convenience we expand around $c_0 = (c_1 + c_2)/2$, with $\delta c = c - c_0$. Since f depends explicitly on c only at linear order and implicitly through v, we expand formally as

$$f = f_0 + \frac{\partial f}{\partial c}\delta c + \frac{\partial f}{\partial v}\delta v + \frac{\partial^2 f}{\partial c\,\partial v}\delta c\,\delta v + \frac{1}{2}\frac{\partial^2 f}{\partial v^2}\delta v^2 + \ldots \tag{12}$$

Now we explicitly evaluate the coefficients. The mixed partial derivative only involves the first term of f because of the c dependence there; using the equation of state, we have

$$\frac{\partial^2 f}{\partial c\,\partial v} = -\frac{\partial p}{\partial c} = -\frac{1}{c}\left(p + \frac{\epsilon}{v^2}\right) \approx -\frac{\epsilon}{c_0 v^2} \tag{13}$$

(In the last approximation, we have dropped the external pressure as negligible compared to the cohesive energy density and put $c \to c_0$ because we are expanding in δc only to second order.)

For the second derivative with respect to v we have

$$\frac{\partial^2 f}{\partial v^2} = -\frac{\partial p}{\partial v} = \frac{1}{v\kappa_T} \tag{14}$$

where $\kappa_T = -(1/v)(\partial v/\partial p)_T$ is the isothermal compressibility.

Now write formally the expansion as

$$g = g_0 + A\delta c + B\delta c\,\delta v + (C/2)\delta v^2 \tag{15}$$

in which we have transformed from Helmholtz to Gibbs free energy (and immediately canceled the pressure term against the derivative $\partial f/\partial v$). This we minimize with respect to δv to obtain

$$\delta v = -(B/C)\delta c \tag{16}$$

The corresponding minimized value of g is

$$g_{\min} = g_0 + A\delta c - \frac{B^2}{2C}\delta c^2 \tag{17}$$

Recalling our results for the partial derivatives, we have

$$\delta g = g_{\min} - g_0 = A\delta c - \frac{\Pi^{*2}\kappa_T v^*}{2}\left(\frac{\delta c}{c_0}\right)^2 \tag{18}$$

in which we have approximated v by v^*.

We can replace the compressibility β in terms of the thermal expansion coefficient α by means of thermodynamic identities, as follows. We have $\alpha = (1/v)(\partial v/\partial T)_p$; then the total derivative $dv = (\partial v/\partial T)_p\, dT + (\partial v/\partial p)_T\, dp$ implies

$$\frac{\alpha}{\kappa_T} = \left(\frac{\partial p}{\partial T}\right)_v \tag{19}$$

Now we evaluate the pressure derivative from the equation of state, eq 11. The temperature derivative only involves the first term, so we have

$$(\partial p/\partial Tt)_v = (p + \epsilon/v^2)/T \approx \epsilon/(Tv^2) \tag{20}$$

where we have as before taken the internal pressure much larger than p itself. Thus, we have finally

$$\frac{\alpha}{\kappa_T} \approx \frac{\Pi^*}{T} \tag{21}$$

Now we compute the free energy of mixing, $\Delta g = \delta g(\phi) - \phi\delta g(1) - (1-\phi)\delta g(0)$. The terms linear in δc cancel altogether, while the terms quadratic in δc give

$$\Delta g = \frac{\Pi^*\alpha T v^*}{2}\left(\frac{c_1 - c_2}{c_0}\right)^2 \phi(1-\phi) \tag{22}$$

We see that if $c_1 = c_2$, there is no contribution to the mixing free energy (as we have assumed identical cohesive energy densities and hard-core volumes per particle of the two species). This contribution to the mixing free energy can be interpreted as a contribution to the χ parameter, as

$$\delta\chi = \frac{\Pi^*\alpha T v^*}{2k_B T}\left(\frac{c_1 - c_2}{c_0}\right)^2 \tag{23}$$

The contribution to polymer−solvent χ parameter of eq 23 is generic in the sense that it evidently depends on the relative difference in Prigogine parameters, which will generically never vanish since polymer segments have $c = 2$ and solvent segments have $c = 3$.

Let us now estimate the typical size of the contribution to χ. For this purpose we observe that the values for the parameters entering eq 23 do not in fact vary widely, among nonpolar polymers. A typical value for the cohesive energy density would be $\Pi^* = 350$ J/cm^3 and for the solvent (equivalently monomer) volume of $v^* = 100$ cm^3/mol.[16] For the thermal expansion coefficient we take the average of typical solvent and polymer values, or $\alpha = 9.5 \times 10^{-4}$/K. Then at $T = 300$ K, we have $\delta\chi = 0.32$, in more than satisfactory agreement with the rule of thumb of adding 0.34 to the solubility parameter estimate of χ.

Now of course values for Π^*, v^*, α, and T would vary somewhat, and thus the predicted contribution $\delta\chi$ would vary in turn. We do not emphasize here the precise value of 0.32, but rather the generic nature of the mechanism, which evidently leads to a contribution of magnitude in close agreement with experiment.

Simulations

So far, we have established the plausibility of the difference in propensity to explore free volume as a generic origin of repulsive χ values for polymer−solvent systems. However, the above quantitative arguments have their limitations, based as they are on a lattice model that can never be more than heuristic and semiquantitative. So we turn to simulations to explore in a different way the appearance of attractive self-interactions of a chain as a result of the presence of explicit solvent.

The arguments we have made depend only on the bonding of polymeric segments and indeed assumed for simplicity identical volumes and energetic interactions for solvent and polymer segments. Thus, we choose to simulate freely joined chains of hard spheres, among a solvent of identical hard spheres. We can then vary the concentration of solvent spheres from zero up to dense-liquid concentrations, to connect the behavior of a single chain in vacuum and in solution. As for quantities to measure in the simulations, we can study the radius of gyration of single chains in solution as a function of chain length and solvent concentration. And, as we shall describe below, we can extract an effective χ value from a comparison of the radius of gyration as observed, to its value for phantom chains (i.e., without self-avoidance).

Alternatively, we can look directly for induced attractive interactions by measuring the second virial coefficient between bonded hard-sphere dimers among hard-sphere solvent. Again we can observe the decrease in the virial coefficient as the solvent concentration increases and again infer an effective χ value as described below. Our reason for looking at the virial coefficients of dimers rather than extended chains is partly convenience—dimers are smaller than chains, so we can simulate many of them and improve our statistics for $g(r)$. But also, we note that local contacts between chain segments typically consist of two pairs of adjacent beads, dimers, nestled into a nearly close-packed tetrahedral arrangement. So the virial coefficient between dimers may be directly relevant to contacts between chains.

The simulations themselves are straightforward, off-lattice Monte Carlo simulations. Spheres are selected at random for an attempted move. Solvent moves are generated as small displacements in a random direction. Moves of polymer beads are generated respecting the bonding constraints of neighboring beads, which confines the attempted moves for interior monomers to lie along a circle and moves for end beads to lie on the surface of a sphere. If a move does not violate the hard-sphere overlap restriction, it is accepted.

To speed equilibration of the large-scale polymeric configurations, we also generate reptative moves, as follows. From one end of a chain, we find the nearest solvent bead and move it along along the line between its center and the center of the

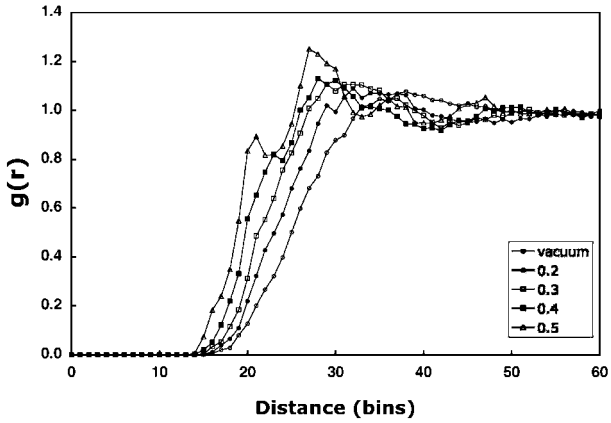

Figure 2. Pair correlation functions $g(r)$ for hard-sphere dimers in vacuum and with $\phi = 0.2$, 0.3, 0.4, and 0.5.

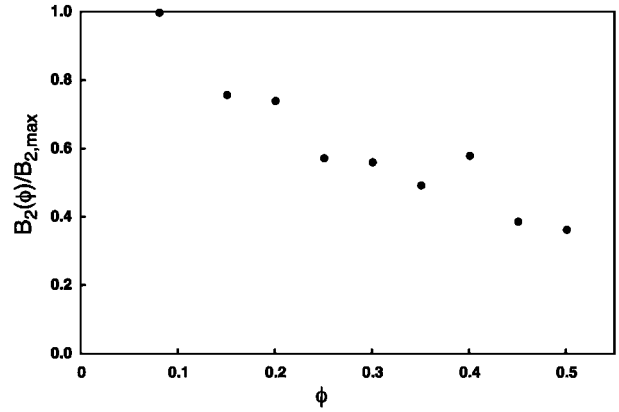

Figure 3. Dimer virial coefficient B_2 versus total volume fraction ϕ, computed from data of Figure 2 using eq 24.

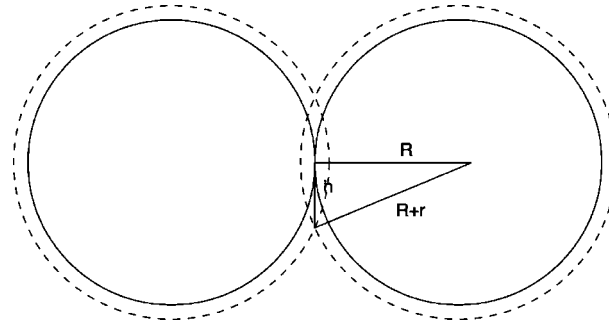

Figure 4. Colloidal particles in contact have overlapping excluded volumes for micelles, thus increasing the available system volume where micelles can visit.

end bead into contact with the end bead, adding a bonding constraint. At the other end of the chain we destroy a bonding constraint. As above, if the move does not violate any overlap restrictions, it is accepted.

We simulated single chains in cubic regions with periodic boundary conditions, with linear dimensions large enough not to perturb the coil dimensions. We simulated chains of length $N = 4$, 8, 16, 32, and 64 beads of unit diameter (with cubic boxes of side length $L = 4$, 6, 8, 12, and 16, respectively). We studied overall bead volume fractions of $\phi = 0.2$, 0.3, 0.4, and 0.5 as well as single chains with no solvent beads ("vacuum") and without hard-sphere overlap constraints ("phantom"). For each system we generated 20 000 configurations, with sufficient MC steps between configurations such that the correlation time for the radius of gyration was no more than 10^{-3} of the total simulation time.

For virial coefficients between dimers, we simulated dimers at a fixed volume fraction 0.08, in vacuum and with added solvent spheres for a total volume fraction of 0.15, 0.2, 0.25, 0.3, 0.35, 0.4, 0.45, and 0.5. For these simulations we used a cubic box of side length $L = 10$ and generated 5000 independent configurations. The virial coefficient is defined as

$$B_2 = (1/2)\int_0^\infty 4\pi r^2(1 - g(r))\mathrm{d}r \tag{24}$$

where $g(r)$ is the pair correlation function between dimer centers (the dimer center being the point of contact between the two spheres of the dimer).

Figure 2 shows the results for $g(r)$ for dimers in vacuum (dimers at 8% volume fraction) and with monomers added to reach a total volume fraction $\phi = 0.2$, 0.3, 0.4, and 0.5. Evidently, the size of the correlation hole for small r decreases as ϕ increases. The corresponding virial coefficient, normalized to that for dimers in vacuum, is displayed in Figure 3. The results are somewhat noisy but the trend is evident, that the virial coefficient has decreased by a factor of about 0.4 from $\phi = 0.08$ to $\phi = 0.5$. Comparing to eq 2, we see this corresponds to a χ value of 0.3 or so.

This encouraging result raises the question of what hard-sphere volume fraction we ought to be comparing to, as the most representative of typical dense liquids. Actual liquids are of course not hard spheres, so how do we map typical liquid densities onto ϕ? We propose choosing ϕ such that the pressure in the hard-sphere liquid is the same as the typical "internal pressure" or cohesive energy density of a real liquid. Real liquids are held together by attractive forces, which give rise to a cohesive energy density far in excess of atmospheric pressure; we may think of the effective "hard core pressure" of a real liquid as just balancing the cohesive energy density.

Now the pressure of hard-sphere liquids is very well described by the Carnahan−Starling equation[29]

$$p(\phi) = \frac{kT}{v}\left(\frac{1 + \phi + \phi^2 - \phi^3}{(1 - \phi)^3}\right) \tag{25}$$

If we take the previously cited typical values of cohesive energy density ($\Pi = 350$ J/cm^3) and solvent volume ($v = 100$ cm^3/mol), then at 300 K we have $\Pi = 14kT/v$. Hence, we seek ϕ such that $p(\phi)$ of eq 25 is likewise about $14kT/v$, which gives $\phi = 0.51$. In fact, hard-sphere liquids undergo a first-order freezing transition at about $\phi = 0.5$, which is not captured by the Carnahan−Starling expression. So we may say that equating internal pressures suggests that the relevant hard-sphere liquid for comparison to real liquids is about as dense as it can be without freezing.

Thinking of the solvent effect on the virial coefficient of hard-sphere dimers suggests an alternative view of the origin of attractive contributions to polymer interactions in solution. We are reminded of the classical theory of depletion interactions induced between micron-sized colloidal particles by nanometer-sized micelles.[30] There, the physical origin of the attraction is as follows. The colloidal particles (of radius R) exclude the centers of the micelles (of radius $r \ll R$) from approaching any closer than r to the surfaces of the particles. Each particle in isolation therefore has an excluded region of volume $4\pi R^2 r$ into which micelle centers cannot go. When two colloidal particles touch, their excluded regions overlap, increasing the volume in the system where micelle centers can travel by an amount ΔV of $2\pi r^2 R$ (see Figure 4). The osmotic pressure Π of the micelles therefore does work $\Pi\Delta V$ as the colloidal particles come into

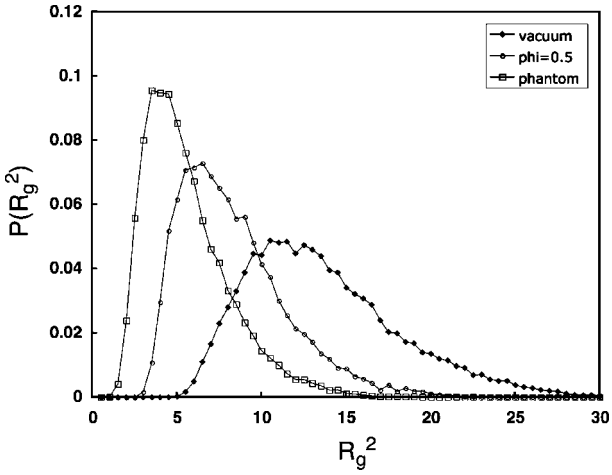

Figure 5. Histogram of the square radius of gyration for a single chain of length $N = 32$ without hard-sphere solvent ("vacuum"), with hard-sphere solvent at total $\phi = 0.5$, and without overlap constraints ("phantom").

contact, resulting in an attractive force between colloidal particles.

Of course, if the colloidal particles are taken to be the same size as the micelles, the argument breaks down; it cannot make sense for identical "red" particles in a sea of "blue" particles to feel an induced attraction due to depletion attractions. But dimers are geometrically unlike single hard spheres. In particular, when a pair of such dimers cluster together into a tetrahedron, they reduce the sum of their excluded volumes by about $5.67\Omega_0$, where Ω_0 is the volume of one hard sphere. Whereas, when two single hard spheres come into contact, they reduce the sum of their excluded volume to other spheres by only about $2.48\Omega_0$. So it is reasonable to expect that dimers, and hence freely jointed hard-sphere chains, will experience significant depletion attractions in the presence of hard-sphere solvent (as is evident in Figure 3).

Results for chain radii of gyration as a function of chain length and solvent volume fraction are also consistent with a reduction of excluded volume parameter. Figure 5 shows a set of histograms for the square radius of gyration of a chain of length $N = 32$ under three conditions: "vacuum" (no added solvent), $\phi = 0.5$, and "phantom" (no overlap penalty). The chain dimensions in solution are evidently smaller than in vacuum; indeed, for the case shown, R_g^2 for $\phi = 0.5$ is about midway between the vacuum (maximally self-avoiding) and phantom (non-self-avoiding) limits.

Figure 6 presents a log−log plot of average values of R_g^2 versus chain length N, for a chain in vacuum, $\phi = 0.2$, 0.3, 0.4, and 0.5, and phantom chains. Here $R_{g0}^2 = N/6$ is the square radius of gyration result for long freely jointed phantom chains, shown as the dashed line. The solid lines shown have the theoretical limiting exponent of self-avoiding chains, $\nu = 0.588$.

We see that the self-avoiding scaling is only approached slowly. For a chain with stronger swelling (vacuum and smaller ϕ values) the simulation results attain the expected self-avoiding random walk scaling at progressively larger N. It appears that self-avoiding scaling is eventually achieved for all values of ϕ, albeit with a smaller prefactor at larger ϕ values; certainly even at $\phi = 0.5$ a chain is swollen with respect to the dimensions it would have with no self-avoidance.

Our results for dimensions of single freely jointed hard-sphere chains in identical hard-sphere solvent as a function of volume fraction are in general agreement with previous simulation results of Escobedo and de Pablo,[31] Grayce,[32] and integral equation results of Taylor and Lipson.[33] Escobedo and de Pablo

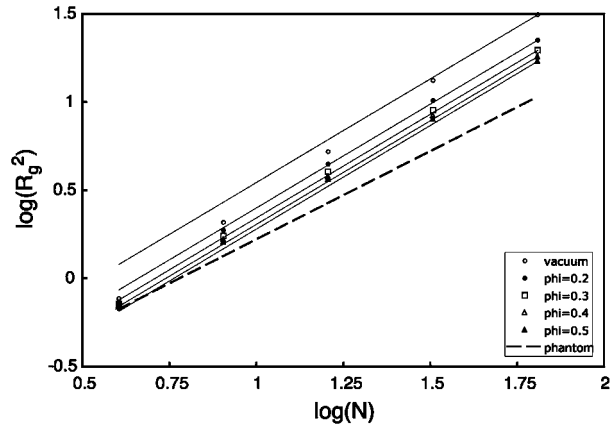

Figure 6. Ratio R_g^2 versus chain length N, for chains in vacuum, with $\phi = 0.2$, 0.3, 0.4, and 0.5, and without overlap constraints (dashed line).

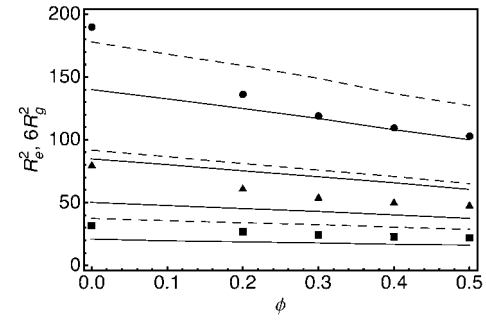

Figure 7. Simulation results of present work for $6R_g^2$ versus volume fraction ϕ for $N = 16$ (squares), 32 (triangles), and 64 (circles). Solid curves are predictions of $R_e^2(N,\phi)$ of ref 33 for $N = 10$, 20, 30, and 50. Dashed curves are interpolated predictions for $N = 16$, 32, and 64.

presented results for radius of gyration for single chains of lengths up to $N = 32$ mers, in vacuum and in hard-sphere solvents of volume fractions ranging from $\phi = 0.2$ to $\phi = 0.48$. Unfortunately, almost all of their results are for chain and solvent mers of different diameters—they observe that smaller solvent mers lead to more swollen chains, as one expects.

Taylor and Lipson's results, based on Born−Green−Yvon integral equation theory, account well for the few data points of ref 31 for equal-sized solvent and chain mers (namely, N ranging up to $N = 32$ and $\phi = 0.2$ or vacuum; see their Figure 8); see Figure 2 of ref 33. We have interpolated the predictions of ref 33 for the mean-square end-to-end distance R_e^2 (which are nearly linear in ϕ as well as N) to generate "predicted" mean-square end-to-end distances for $N = 16$ and $N = 32$ as a function of ϕ. These are shown in Figure 7 together with our simulation results, which we have heuristically converted from mean-square gyration radii to mean-square end-to-end distances by multiplying by 6.

Evidently, while there is reasonable qualitative agreement between our results for gyration radii so "converted" to end-to-end distances and the predictions of ref 33, the agreement is not quantitative. This is likely because of the approximate nature of the relation we have used to convert R_g^2 to R_e^2, namely $R_e^2 = 6R_g^2$. This proportionality constant is only exactly 6 for random walks and may be expected to vary as the degree of swelling varies with changing N and ϕ. The important conclusion to be drawn about the behavior of the radius of gyration with solvent fraction is the extent to which the chain dimensions decrease, and the degree of decrease we observe is roughly in accord with previous results and predictions.

From such data as presented in Figure 6, we can extract an estimate of the effective value of w and hence χ by making use

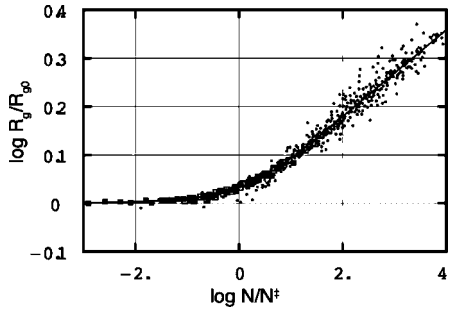

Figure 8. Swelling crossover master curve, R_g^2/R_{g0}^2 vs $N/N^{\ddagger}$, obtained from data (small points) and simulation results (closed and open squares) as described in text. Solid curve is solution of eq 26.

of the swelling crossover curve.[34] In eq 4 we reprised Flory's simple result for how the chain dimension crosses over from Gaussian random-walk scaling, appropriate to a chain in melt or Θ-solution conditions, to self-avoiding scaling, appropriate to good-solvent conditions. This behavior has been explored experimentally by measuring for many polymer−solvent systems the chain length dependence of chain dimensions in the melt (or, equivalently, in Θ-solvents) and in solution. Results were plotted log−log as R_g^2/R_{g0}^2 vs $N/N^{\ddagger}$, in which the value of $N^{\ddagger}$ for each polymer−solvent system was chosen to collapse all the data on a master curve.

Simulations were also performed with a tethered-bead polymer model with an adjustable truncated Lennard-Jones potential between beads. The adjustable truncation allowed for adjustment of the strength of the attractive well between beads and thereby the variation of the solvent quality. The Θ-point was located, corresponding to a particular truncation of the LJ potential; then, different "good solvent" conditions (potentials less attractive than Θ-condition) and chain lengths were explored.

The results so produced were likewise collapsed onto the same master curve as the above-mentioned experimental data. The master curve is well fit by the solution of an expression inspired by eq 4

$$(R/R_0)^{5.59} - (R/R_0)^{-9.43} = (N/N^{\ddagger})^{1/2} \qquad (26)$$

In eq 26, the exponent 5.59 (originally 5 in eq 4) has been adjusted to produce the best theoretical value for the swelling exponent (that is, $5.59 = 1/(2\nu - 1)$, with $R \sim N^{\nu}$ in good solvent conditions). The second term (exponent −9.43) has been adjusted arbitrarily to produce the best description of the observed crossover. Evidently, this value is a long way from the result of the Flory argument. The corresponding crossover curves, however, are very similar. The reason is that the crossover pertains only to good solvents, for which $R \geq R_0$; the crossover is to $R/R_0 = 1$ as $N^{\ddagger}/N \to \infty$. The experimental and simulation results together with the solution of eq 26 are shown in Figure 8.

We can use the crossover curve to extract a value of $N^{\ddagger}$, by computing the ratio R_g^2/R_{g0}^2 from our simulations for chains of a given N and a given ϕ, finding the corresponding value of $N/N^{\ddagger}$ from the crossover curve, and using the known value of N to infer $N^{\ddagger}(\phi)$. We may use the same procedure to extract a minimum value of $N^{\ddagger}(0)$ from the results for chains in vacuum. Then, using the scaling of $N^{\ddagger}$ as w^{-2} (eq 34), we can infer the ratio $w(\phi)/w(0)$.

For example, for $N = 64$, the ratio R_g/R_{g0} for a chain in vacuum is $\exp((1.4996 - 1.028)/2) = 1.266$ and for $\phi = 0.5$ is $\exp((1.2355 - 1.028)/2) = 1.109$; for $N = 32$, we have the corresponding ratios as $\exp((1.127 - 0.727)/2) = 1.221$ and $\exp((0.9063 - 0.727)/2) = 1.094$. Consulting Figure 8, we find

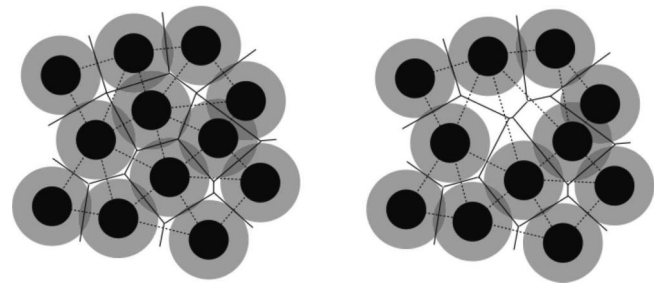

Figure 9. Definition of free volume from ref 35. The center of a given particle is free to traverse the contiguous area containing its center, outside the overlap region of other particles. The area is made visible by removal of the particle (right).

for $N = 64$ that $N/N^{\ddagger}$ equals 13.1 for chains in vacuum and 1.97 for $\phi = 0.5$; for $N = 32$ the corresponding values are 8.38 and 1.49. [Thus, for chains in vacuum we find $N^{\ddagger} \approx 4$ monomers, which is a small and therefore reasonable value—dependent on our conventions regarding factors of order unity in eq 33.] From the $N = 64$ results we find w has been reduced from vacuum to $\phi = 0.5$ by a factor of $(13.1/1.97)^{1/2} = 2.58$; the corresponding value from the $N = 32$ results is 2.37.

Recalling eq 2, we see that a reduction of w by a factor of f from the value in vacuum (where for single hard-sphere chains we have $\chi = 0$ by definition), we can infer a value of χ of $(1 - f)/2$. Thus, the above results translate to $\chi = 0.306$ and $\chi = 0.289$, respectively. Hence, we say that our results for the reduced chain dimensions in concentrated hard-sphere solvents are consistent with a value of χ of about 0.3.

Free Volume

Our off-lattice MC simulations give results for effective χ values from dimer virial coefficients and chain dimensions that are consistent with our analytical arguments from the cell model. The cell model was built upon a notion of "free volume" that we now explore with the help of the simulation results, where cells are not a feature ab initio of the hard-sphere chain model.

Sastry and co-workers have presented a precise definition of free volume in hard-sphere systems and developed a sophisticated algorithm to evaluate it from hard-sphere configurations.[36,37] Their definition of the free volume of a given sphere in a given configuration is the following: the volume over which the center of the given sphere may be continuously translated without overlapping another sphere, while holding fixed the positions of all other spheres in the configuration. (Note that Sastry's definition of free volume is a "one-particle" statistical property, as it involves the moving of one particle in a configuration with all other particles fixed, and the value will depend on which particle is chosen from what configuration.) Figure 9 illustrates this definition.

The Sastry et al. algorithm begins with a Voronoi tesselation of the space inhabited by the particles, for which a variety of algorithms have been presented.[36,37] Note that their definition of free volume is *not* equivalent to that most commonly used (and most conveniently calculated), which is simply the difference between the volume of a particle's Voronoi cell and the particle volume itself. Sastry's definition, in a one-particle sense, captures the essence of configurational entropy, in counting the number of places a particle can be put without "rearranging" cages or "exchanging" particles.

Reference 39 presents probability distributions of free volume for different hard-sphere concentrations, corresponding to volume fractions $\phi = 0.419$, 0.445, 0.471, 0.476, 0.487, and 0.494. Representative results are shown in Figure 10.

The distributions $P(v_f)$ are very well described by a phenomenological function of a form suggested by Hoover[38]

$$P(v) \sim v^{\alpha} \exp(-Av^{\gamma}) \tag{27}$$

in which the exponents α and γ, and the coefficient A, are fitting parameters. The exponents reported by Sastry et al. are found to vary with ϕ over a relatively narrow range, yielding α in the range 0.28−0.35 and γ in the range 0.55−0.45 as ϕ increases over the range studied.[39]

Evidently, the distribution of free volume values is broad, with a sharp decay for sufficiently large v_f and significant probability of even very small v_f values. As the density increases, the distributions shift progressively toward smaller v_f, as one expects. No explanation has been presented for the appropriateness of the form eq 27 or the values of the parameters.

We have employed the Sastry algorithm to compute free volume distribution functions for both solvent and chain spheres in our off-lattice MC simulations. We are interested to see whether the idea of our cell model, that the chain segments would have less free volume than solvent spheres, is borne out in the simulation results. As well, we have extended the range over which the distribution functions are known, by working at higher precision and collecting more values. This is important to pin down the values of the exponents in the Hoover function, as we shall see.

First, we consider results for hard spheres without chains present. Figure 11 displays the histograms of free volume in a system of hard spheres with $\phi = 0.37$, 0.39, 0.42, 0.45, 0.47, 0.50, 0.52, 0.55, 0.58, 0.60, and 0.63.

Our histograms are computed from equally spaced bins in log v_f; that is, we evaluate directly a discretized approximation to the normalized probability distribution for log v_f, which we denote $\tilde{P}(\log v_f)$. This enables us to extend our distributions to smaller values of v_f than would be possible with a linear bin spacing. To convert this to the usual probability distribution for v_f, we use the normalization requirement $\tilde{P}(\log v_f)\, d(\log v_f) = P(v_f)\, dv_f$, which implies $\tilde{P}(\log v_f) = v_f P(v_f)$. Thus, in Figure 11 we have actually plotted $\tilde{P}(\log v_f)/v_f$ (on a log scale) vs log v_f.

Note that there is a distinct change in the shape of the distributions for volume fractions above the freezing point (approximately $\phi = 0.5$). For these higher volume fractions, the distribution is more narrow than for the lower (liquid) volume fractions.

Figure 12 displays the free volume distribution for chain mers of a single chain in a hard-sphere liquid at overall volume fraction $\phi = 0.5$, compared to the free volume distribution of solvent mers in the same system. We observe that the average v_f is smaller for chain mers than for solvent mers; for the data shown, the average values of v_f for solvent mers and chain mers are 0.0046 and 0.0019, respectively. Further, the distribution for chain mers is not the same shape as that for solvent mers—relatively small values of v_f figure more prominently in the distribution for chain mers than for solvent mers. Qualitatively, we expect such a result from the physical idea of our cell model.

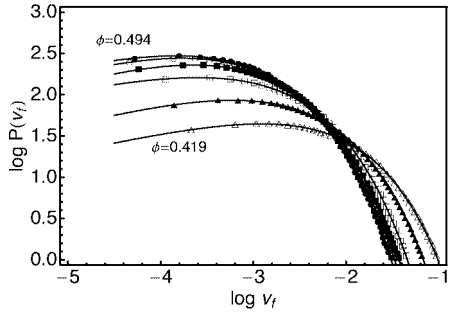

Figure 10. Probability distribution of free volume for $\phi = 0.419$, 0.445, 0.471, 0.476, 0.487, and 0.494 from ref 39. Solid curves are fits to eq 27.

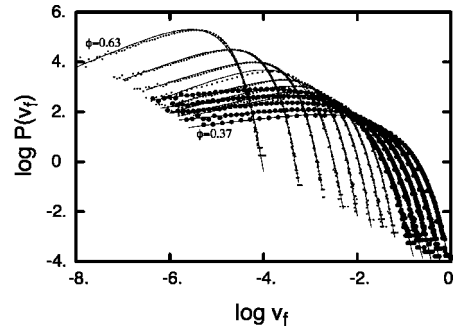

Figure 11. Probability distribution of free volume for hard-sphere fluids with $\phi = 0.37$, 0.39, 0.42, 0.45, 0.47, 0.50, 0.52, 0.55, 0.58, 0.60, and 0.63 from present work. Solid curves are fits to eq 27.

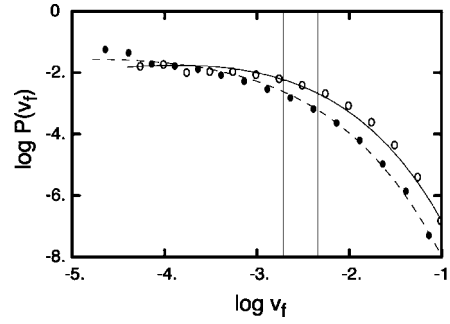

Figure 12. Probability distribution of free volume for chain mers (filled symbols) and solvent mers (open symbols) in a system consisting of a single chain of $N = 16$ mers in a total volume fraction of $\phi = 0.5$. Solid (solvent) and dashed (chain) curves are fits to eq 27, with exponent values $\gamma = 1/3$ for both solvent and chain mers and $\alpha = 2/3$ for solvent mers and 1/3 for chain mers (see discussion in text).

Cell Model Result for $P(v_f)$

Now, we present an argument for the shape of this distribution, inspired by the cell model. Consider a single hard sphere in a hard-sphere liquid at some reasonably high density, such that typical particles are all "caged" and the free volume of particles are small compared to their geometrical volumes. What controls the likelihood that a given particle will have an unusually large free volume? For this to occur, neighboring particles will be obliged to keep a bit further away from the given particle, enlarging its Voronoi cell. We may think of this particle as occupying a cell, as in the cell model, but with fluctuating volume. When the cell becomes larger, the particle has more free volume and hence more configurational entropy; but to enlarge the cell, work must be done against the osmotic pressure of the surrounding fluid.

This motivates us to write an effective free energy for the single-particle system, in equilibrium with the surrounding fluid as a pressure bath, as

$$f = -\frac{c}{3} kT \log v_f + p(\phi) v \tag{28}$$

in which $p(\phi)$ is the pressure of the hard-sphere fluid, v the cell volume, v_f the free volume, and c as before the number of translational degrees of freedom per particle.

Fluctuations of the cell dimensions are then controlled by a Boltzmann factor constructed from this free energy, whereupon the probability of finding a given value of v_f is

$$P(v_f) = \int dx\, dy\, dz\, \delta(v_f - \Delta x \Delta y \Delta z) \exp(-\beta f) \tag{29}$$

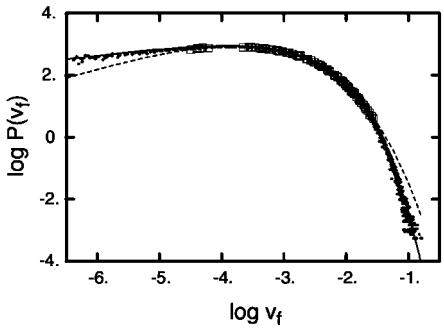

Figure 13. Master curve for the free volume histograms for "dense fluids" (here, $0.4 \leq \phi \leq 0.5$). Large open squares are simulation results of Sastry et al.; small filled points are present work. Dashed curve is fit of form eq 27 with exponents $\alpha = 2/3$ and $\gamma = 1/3$ as in eq 30. Solid curve is fit of form eq 27, but with adjusted exponents $\alpha = 0.25$ and $\gamma = 0.5$.

Here we have adopted the simple cubic geometry of our cell model, allowing the cell dimensions x, y, and z to fluctuate independently. $\Delta x = x - d$ is the difference between the cell dimension and the diameter of the particle; the particle center can translate over a distance Δx in the x-direction.

We evaluate eq 29 in the limit of large pressures $p(\phi)$, i.e., in the approximation that v_f is much smaller than v. This allows us to expand v in the exponent around the close-packed limiting value $v^* = d^3$, to first order in the displacements Δx, Δy, and Δz. The delta function constrains the integral to a surface. The point with $\Delta x = \Delta y = \Delta z$ minimizes the exponent subject to the constraint, and we expand about this point to second order in displacements along the constraint surface to evaluate the integral for large $p(\phi)$. After some arithmetic we obtain

$$P(v_f) \sim v_f^{2/3} \exp(-3\beta p(\phi) v^{*2/3} v_f^{1/3}) \tag{30}$$

Thus, we find the form of eq 27, but with concrete predictions that $\alpha = 2/3$, $\gamma = 1/3$, and $A = 3\beta p(\phi) v^{*2/3}$.

We have observed that, for a range of densities $0.4 \leq \phi \leq 0.5$ such that most particles are caged but the system remains fluid, Sastry's and our results for the hard-sphere fluid free volume distribution are essentially unchanged in shape. We can thus assemble a master curve from the histograms for volume fractions in this range by shifting horizonally and vertically on a log−log plot. For definiteness, we choose to shift all the data onto the histogram for dense fluids just below freezing, at $\phi = 0.5$.

In Figure 13 we compare the master curve so generated to the Hoover function with exponents given by eq 30 (dashed curve). The agreement is reasonable given the simplicity of the model. For the Sastry data (larger open squares, for log v_f ranging from about −4.5 to −1.5), one would conclude the exponents of eq 30 account perfectly for the histogram. However, for our more extensive range of v_f values, it is evident that these exponent values are not quite right. The small-v_f power-law behavior is better fit by $\alpha = 0.25$ rather than 2/3, and with this value fixed the entire histogram is well accounted for by $\gamma = 0.5$ rather than 1/3. A fit based on these adjusted exponent values is shown as the solid curve in Figure 13.

The coefficient A and thus the horizontal shift factors required to place the theory on the data are likewise reasonably accounted for by our simple argument. In Figure 14 we plot the values of the coefficient A taken as a fitting parameter to fit the data in Figure 11, versus the predicted value of A from eq 30 (in which we have used the Carnahan−Starling result (eq 25) for the pressure). We find a consistent trend with ϕ relative to the data, with the ratio of the predicted and extracted A values being very nearly a constant 0.88.

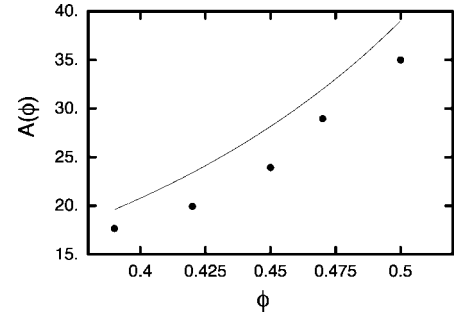

Figure 14. Values of coefficient A from eq 27, as extracted from fits to data of Figure 11 (points) and predicted from eq 30 (solid curve).

Finally, we consider the cell-model argument for the form of $P(v_f)$ for a bonded chain mer as opposed to a free solvent hard sphere. Because of the lesser number of degrees of freedom for the bonded mer, we have $c = 2$ instead of $c = 3$, which ultimately gives rise to $\alpha = 1/3$ instead of 2/3. The histogram for free volume of chain mers shown in Figure 12 is fit to the result of eq 27 with this value of α, which roughly captures how the shape of the histogram differs from that for the solvent mers.

We have not gathered as extensive a set of results for the free volume distribution for chain mers as we have for solvent mers. To do so would be challenging because of the computer time required to apply the Sastry algorithm to a sufficient number of configurations to get good statistics, of a simulation volume large enough to contain a chain and otherwise full of solvent. Much smaller simulation volumes can be used when one seeks the free volume distribution for solvent mers only.

Presumably, more extensive results would likewise show that the precise values of the Hoover exponents that fit the free volume distribution for chain mers are not given by our simple argument, just as it was found for solvent mers. However, the simple argument does predict the trend in the free volume distribution as we compare solvent mers and chain mers, namely, that the distribution for chain mers has more prominent contributions from relatively small free volumes. It may be possible to elaborate our simple argument with a more realistic geometry for the cavity volume than that of a rectangular parallelpiped with a cube-shaped particle inside, an improvement we leave to future work.

Conclusions

We have shown that the bonding constraints acting on the mers in a polymer chain reduce the propensity of those mers to explore free volume, when compared to a liquid of unbonded but otherwise identical spheres. This generic difference in affinity for free volume of polymer chains versus solvent leads to a positive contribution to the free energy of mixing, as the mixture compromises to determine its density, by minimizing the sum of contributions from the cohesive energy and the configurational entropy.

Within a simple cell model of the type introduced by Flory, Orwall, and Vrij, we have shown that the difference in affinity for free volume for chains versus solvent leads to a contribution to χ proportional to the difference in Prigogine parameters (which count the number of degrees of freedom per particle) and will thus be generically nonzero. Using typical values of volume per mer and cohesive energy density, we have shown that the resulting contribution to χ is about 0.3, consistent with the observed rule of thumb for good nonpolar solvents of nonpolar polymers. This generic contribution is absent for polymer blends, thus permitting extremely small values of χ for pairs of nonpolar polymers with matched solubility parameters.

Our off-lattice Monte Carlo simulations of hard-sphere freely jointed chains and identical hard-sphere solvent illustrate directly the generic effects of the chain bonds on polymer−solvent interactions. We have observed that hard-sphere dimers in concentrated hard-sphere solvent show a reduced virial coefficient, of a magnitude consistent with the generic value of χ found above. Also, we have observed directly the reduced chain dimension of single chains in hard-sphere solvent relative to vacuum, again consistent with a χ value of about 0.3.

Using the definition and algorithm of Sastry et al. for free volume of a hard-sphere system, we have extracted from our simulations the distribution of free volumes $P(v_f)$ for solvent spheres and chain mers. Our results for solvent agree with those of Sastry et al. and extend their results to a greater range of v_f (1 decade larger and 2 decades smaller values).

Our results for $P(v_f)$ are well fit by a phenomenological function proposed by Hoover, with $\alpha = 0.25 \pm 0.03$ and $\gamma = 0.51 \pm 0.02$. Because of the wider range of v_f in our histograms, the error bars on α and γ are somewhat tighter than can be determined from the Sastry results, which are consistently fit with $\alpha = 0.35 \pm 0.07$ and $\gamma = 0.44 \pm 0.04$. Our simulations show that the free volume for chain mers is indeed less than for solvent spheres, with a distribution also well described by the Hoover function, with different values for the exponents α and γ.

Finally, we construct the probability distribution of free volume for solvent spheres or chain mers, based on a calculation of fluctuations of a single cell in a cell model of the type introduced by Flory, Orwoll, and Vrij. We derive the Hoover expression, with predictions for its three fitting parameters. The resulting form is in reasonably good agreement with simulation results, including both the exponent values and the dependence on solvent volume fraction, for the free volume distributions of both solvent and chain mers. However, the best values for exponents extracted from fitting the Hoover function to our free volume distributions—approximately $\alpha = 1/4$ and $\gamma = 1/2$ for the case of solvent mers—do not agree with the predictions of our simple model ($\alpha = 2/3$ and $\gamma = 1/3$ for solvent mers). This disagreement may be due to the oversimplified geometry of the cell model, refinements of which we leave to future work.

Acknowledgment. We thank Sharon Glotzer and Gary Grest for helpful and enjoyable conversations.

Appendix

The classic account of chain dimensions in dilute solution was given by Flory, who wrote a mean-field expression for the free energy of a single chain in solution.[14] We summarize his argument in terms of a single-chain free energy

$$\beta F = \frac{3R^2}{2R_0^2} - \log\left(\frac{R^3}{R_0^3}\right) + \frac{wN^2}{2R^3} \tag{31}$$

in which R_0 is the Gaussian end-to-end distance of a chain of N segments and R is the coil dimension to be determined by minimizing F. (The first two terms in F represent the entropy of a random walk with end-to-end vector within a sphere of radius R; the last term is a random-mixing estimate of the excluded volume interaction of the chain with itself.)

Minimizing F of eq 31 gives

$$(R/R_0)^5 - (R/R_0)^3 = R_0/(2l_s) = (1/2)(N/N_s)^{1/2} \tag{32}$$

in which we have defined the swelling length l_s (sometimes called the "thermal blob size"), the swelling volume fraction ϕ_s, and the swelling chain length N_s by the relations

$$l_s^2 = N_s b^2 \tag{33a}$$

$$wN_s\phi_s/\Omega_0 = 1 \tag{33b}$$

$$\phi_s = N_s\Omega_0/l_s^3 \tag{33c}$$

The meaning of the above relations and the resulting swelling length is this: a small enough portion of a polymer chain in solution will exhibit configurations of an unperturbed Gaussian random walk because it will not have sufficient self-interactions to avoid itself by swelling. A polymer of chain length N_s, with end-to-end distance l_s (eq 33a) and excluded volume parameter w, will have about kT of self-interaction (eq 33b) with the average composition ϕ_s within its own coil volume (eq 33c). Chains longer than N_s will be able to reduce their free energy by swelling to avoid self-interactions.

For chains smaller than N_s, the right-hand side of eq 32 is negligible, and the coil dimension R is equal to the unperturbed dimension R_0. For chains larger than N_s, the right-hand side of eq 32 becomes large, so that R well exceeds R_0 and the second term in eq 32 may be neglected. Self-avoidance thus leads to excluded volume scaling for the chain dimension:

$$\left(\frac{R}{R_0}\right)^2 \sim \left(\frac{N}{N_s}\right)^{2\nu-1}$$
$$N_s \sim (b^3/w)^2 \tag{34}$$

Here ν is the exponent such that R scales as N^ν, which from the Flory argument is $\nu = 3/5$; the best accepted value is $\nu = 0.588$ whereupon $2\nu - 1 = 0.176$ (see ref 34 and references therein).

References and Notes

(1) de Gennes, P.-G. *Scaling Concepts in Polymer Physics*; Cornell University Press: Ithaca, NY, 1979.
(2) *Polymer Handbook*, 4th ed.; Brandrup, J., Immergut, E. H., Grulke, E. A., Eds.; Wiley: New York, 1999.
(3) Flory, P. J. *Discuss. Faraday Soc.* **1970**, *49*, 7.
(4) Orwoll, R. A.; Arnold, P. A. Polymer-Solvent Interaction Parameter χ. In *Physical Properties of Polymers Handbook*; Mark, J. E., Ed.; Springer Science: New York, 2007; p 233.
(5) Huggins, M. L. *J. Am. Chem. Soc.* **1942**, *68*, 1712.
(6) Small, P. A. *J. Appl. Chem.* **1953**, *3*, 71.
(7) Blanks, R. F.; Prausnitz, J. M. *Ind. Eng. Chem. Fund.* **1968**, *3*, 1.
(8) Lohse, D. J. *J. Macromol. Sci., Polym. Rev.* **2005**, *C45*, 289.
(9) Hildebrand, J. H.; Scott, R. L. *The Solubility of Nonelectrolytes*, 3rd ed.; Dover Publications: New York, 1964.
(10) Lohse, D. J. *J. Macromol. Sci., Rev.* **2005**, *45*, 289.
(11) Lohse, D. J.; Graessley, W. W. Thermodynamics of Polyolefin Blends. In *Polymer Blends: Formulation and Performance*; Paul, D. R., Bucknall, C. B., Eds.; Wiley: New York, 2000; Vol. *1*, Chapter 8, pp 219−237.
(12) Bates, F. S.; Rosedale, J. H.; Schulz, M. F.; Almdal, K. U.S. Patent 5,710,219, 1998.
(13) Milner, S. T. *Macromolecules* **2005**, *38*, 4929.
(14) Flory, P. J. *Principles of Polymer Chemistry*; Cornell University Press: Ithaca, NY, 1953.
(15) Patterson, D. *J. Polym. Sci., Part C* **1968**, *16*, 3379.
(16) Graessley, W. W. *Polymeric Liquids and Networks: Structure and Properties*; Garland Books: New York, 2004.
(17) *Handbook of Chemistry and Physics*, 81st ed.; Lide, D. R., Ed.; CRC Press: Boca Raton, FL, 2000.
(18) As a result, the mass density and the cohesive energy density would be expected to be slightly higher for polymer melts than for corresponding monomeric or oligomeric liquids. However, because the free volume is typically such a small fraction of the "hard-core" volume (i.e., of the liquid with negligible free volume, at very low temperatures), this expected difference between polymers and solvents is not so pronounced as the disparity in thermal expansion coeffients.
(19) Prigogine, I. N. *The Molecular Theory of Solutions*; North-Holland: Amsterdam, 1957.
(20) Flory, P. J.; Orwoll, R. A.; Vrij, A. *J. Am. Chem. Soc.* **1964**, *86*, 3507.
(21) Flory, P. J.; Orwoll, R. A.; Vrij, A. *J. Am. Chem. Soc.* **1964**, *86*, 3515.
(22) Flory, P. J. *J. Am. Chem. Soc.* **1965**, *87*, 1833.
(23) Booth, C.; Devoy, C. L. *Polymer* **1971**, *12*, 309.
(24) Booth, C.; Devoy, C. L. *Polymer* **1971**, *12*, 320.

(25) Schreiber, H. P.; Tewari, Y. B.; Patterson, D. *J. Polym. Sci.* **1973**, *11*, 15.
(26) Allen, G.; Gee, G.; Wilson, G. J. *Polymer* **1960**, *1*, 456.
(27) Orwoll, R. A.; Flory, P. J. *J. Am. Chem. Soc.* **1967**, *89*, 6814.
(28) Zeberg-Mikkelsen, C. K.; Baylaucq, A.; Barrouhou, M.; Boned, C. *Phys. Chem. Chem. Phys.* **2003**, *5*, 1547.
(29) Carnahan, N. F.; Starling, K. E. *J. Chem. Phys.* **1969**, *51*, 635.
(30) Witten, T. A.; Pincus, P. *Structured Fluids: Polymers, Colloids, Surfactants*; Oxford University Press: Oxford, UK, 2004.
(31) Escobedo, F. A.; de Pablo, J. J. *Mol. Phys.* **1996**, *89*, 1733.
(32) Grayce, C. J. *J. Chem. Phys.* **1997**, *106*, 5171.
(33) Taylor, M. P.; Lipson, J. E. G. *Fluid Phase Equilib.* **1998**, *150*−*151*, 641.
(34) Graessley, W. W.; Hayward, R. C.; Grest, G. S. *Macromolecules* **1999**, *32*, 3510.
(35) Sastry, S.; Corti, D. S.; Debenedetti, P. G.; Stillinger, F. H. *Phys. Rev. E* **1997**, *56*, 5524.
(36) Taemura, M.; Ogawa, T.; Ogita, N. *J. Comput. Phys.* **1983**, *51*, 191.
(37) Okabe, A.; Boots, B.; Sugihara, K.; Chiu, S. N. *Spatial Tessellations: Concepts and Applications of Voronoi Diagrams*; John Wiley: Chichester, 2000.
(38) Hoover, W. G.; Hoover, N. E.; Hanson, K. *J. Chem. Phys.* **1979**, *70*, 1837.
(39) Sastry, S.; Truskett, T. M.; Debenedetti, P. G.; Torquato, S.; Stillinger, F. H. *Mol. Phys.* **1998**, *95*, 289.

MA801091B